Bariatric surgery improves postprandial VLDL kinetics and restores insulin-mediated regulation of hepatic VLDL production

Vehpi Yildirim, … , Natal A.W. van Riel, Geesje M. Dallinga-Thie

Research Article **Metabolism**

Graphical abstract

Bariatric surgery improves postprandial VLDL kinetics and restores insulin-mediated regulation of hepatic VLDL production
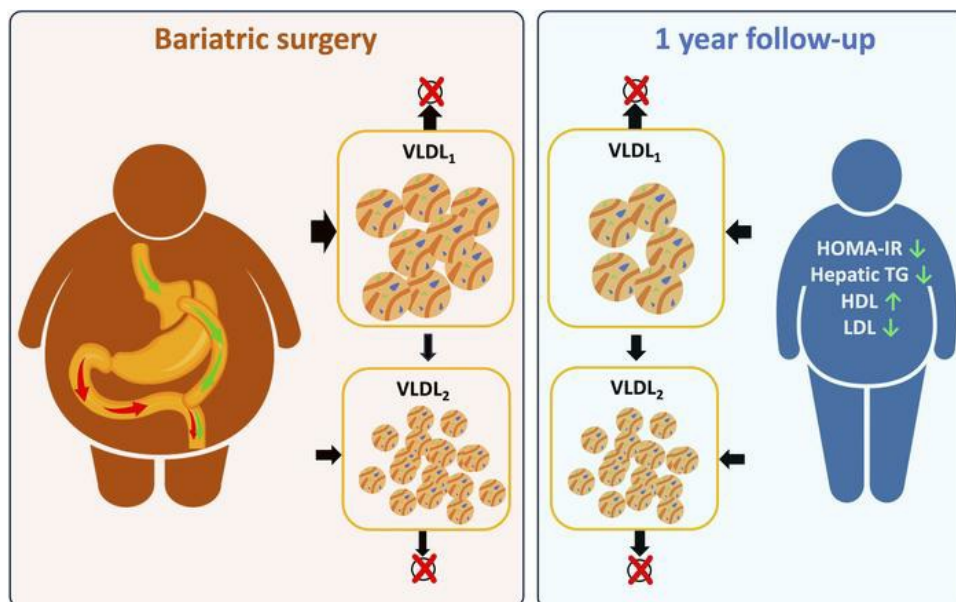
Vehpi Yildirim,[1,2] Kasper W. ter Horst,[3] Pim W. Gilijamse,[3] Dewi van Harskamp,[4] Henk Schierbeek,[4] Hans Jansen,[4] Alinda W.M. Schimmel,[4] Max Nieuwdorp,[4] Albert K. Groen,[4] Mireille J. Serlie,[3] Natal A.W. van Riel,[4,5] and Geesje M. Dallinga-Thie[4]

[1]Department of Public and Occupational Health, Amsterdam University Medical Centers, Amsterdam, The Netherlands. [2]Department of Mathematics, Erzurum Technical University, Erzurum, Turkey. [3]Department of Endocrinology and Metabolism, and [4]Department of Experimental and Vascular Medicine, Amsterdam University Medical Centers, Amsterdam, The Netherlands. [5]Department of Biomedical Engineering, Eindhoven University of Technology, Eindhoven, The Netherlands.

Dyslipidemia in obesity results from excessive production and impaired clearance of triglyceride-rich (TG-rich) lipoproteins, which are particularly pronounced in the postprandial state. Here, we investigated the impact of Roux-en-Y gastric bypass (RYGB) surgery on postprandial VLDL$_1$ and VLDL$_2$ apoB and TG kinetics and their relationship with insulin-responsiveness indices. Morbidly obese patients without diabetes who were scheduled for RYGB surgery ($n = 24$) underwent a lipoprotein kinetics study during a mixed-meal test and a hyperinsulinemic-euglycemic clamp study before the surgery and 1 year later. A physiologically based computational model was developed to investigate the impact of RYGB surgery and plasma insulin on postprandial VLDL kinetics. After the surgery, VLDL$_1$ apoB and TG production rates were significantly decreased, whereas VLDL$_2$ apoB and TG production rates remained unchanged. The TG catabolic rate was increased in both VLDL$_1$ and VLDL$_2$ fractions, but only the VLDL$_2$ apoB catabolic rate tended to increase. Furthermore, postsurgery VLDL$_1$ apoB and TG production rates, but not those of VLDL$_2$, were positively correlated with insulin resistance. Insulin-mediated stimulation of peripheral lipoprotein lipolysis was also improved after the surgery. In summary, RYGB resulted in reduced hepatic VLDL$_1$ production that correlated with reduced insulin resistance, elevated VLDL$_2$ clearance, and improved insulin sensitivity in lipoprotein lipolysis pathways.

Introduction

The prevalence of obesity has increased alarmingly over the past decades (1). Its associations with cardiovascular disease (CVD) and insulin resistance make obesity a major public health problem. Increased fasting and postprandial plasma triglyceride (TG) concentrations, reduced HDL cholesterol levels, and an increased number of LDL particles are the key characteristics of the dyslipidemia observed in patients with obesity. These lipid abnormalities result from an imbalanced lipoprotein metabolism caused by increased TG-rich lipoprotein (TRL) production and reduced TRL clearance (2, 3). Moreover, the interplay between lipid abnormalities and insulin resistance gives rise to a significantly elevated risk of developing CVD and of premature death in patients with obesity (4–6).

The pathophysiology of dyslipidemia in obesity is attributed to the hepatic overproduction and secretion of apolipoprotein B–containing (apoB-containing) TRLs and their impaired clearance from the circulation (2, 7–9). TRLs transport hydrophobic TG and cholesterol from the intestine and liver to peripheral tissues. The intestine produces and secretes chylomicrons (CMs), whereas liver produces and secretes VLDLs. VLDLs are categorized into 2 subfractions based on their sizes: VLDL$_1$ and VLDL$_2$, where VLDL$_1$ is the larger and transports a greater amount of TG per particle. Although, other than their sizes and TG load, there is virtually no difference between VLDL$_1$ and VLDL$_2$, these VLDL subtypes

exhibit different profiles under certain metabolic conditions. In patients with insulin resistance and/or hepatic steatosis, there is $VLDL_1$, but not $VLDL_2$, overproduction (10, 11). Moreover, hyperinsulinemia suppresses hepatic production of $VLDL_1$ but not $VLDL_2$ in both insulin-sensitive and insulin-resistant humans with low liver fat (12–14).

In target tissue capillaries, TGs in TRLs are hydrolyzed to glycerol and free fatty acids (FFAs) by lipoprotein lipase (LPL), and the products are taken up by tissue cells. As a result, circulating TRLs are transformed into smaller and denser, cholesterol-enriched lipoprotein particles. Because these small lipoprotein particles are enriched in cholesterol, they are highly proatherogenic, and their accumulation in plasma poses a significant risk for development of CVD (15). Many studies have shown a close association between dyslipidemia and the occurrence of insulin resistance and type 2 diabetes (16–19). Many hypotheses have been proposed in the literature to explain this relationship (20), but the molecular mechanism explaining how dyslipidemia, per se, may induce insulin resistance is not fully understood; more importantly, the chicken-or-egg question has not yet been answered.

Bariatric surgery is an effective treatment for patients with severe obesity; it induces sustained weight loss and improves both overall health and quality of life (21, 22). In addition to weight loss, bariatric surgery improves blood glucose regulation, insulin sensitivity, plasma lipid profiles, and BP (23, 24). Because of its high success rate, Roux-en-Y gastric bypass (RYGB) surgery is 1 of the most commonly performed bariatric procedures (25). Notably, RYGB results in dramatic improvements in insulin resistance and dyslipidemia that are not necessarily related to the extent of the weight loss (26–28). Such weight loss–independent effects of bariatric surgery often occur within a few days to weeks after the surgery and may be related to (acute) changes in caloric intake, the microbiome, and/or gastrointestinal hormones (27, 29). However, the concurrent changes that take place after the surgery make it difficult to unravel the line of events that ultimately leads to improved glucose and lipoprotein metabolism.

Computational modeling has proven to be effective for analyzing complex biological systems data and understanding hidden cause-and-effect relations (30, 31). In this regard, several computational models of human lipoprotein metabolism have been developed to analyze stable isotope–labeled tracer data (32–34). In human lipoprotein metabolism studies, tracer techniques usually are used under steady-state (fasting) conditions, where the influx and outflux of the trace are equal and all regulatory elements are assumed to be fixed (35). However, humans spend the majority of their time under nonsteady-state (postprandial) conditions. Moreover, postprandial metabolism is more strongly related to metabolic and cardiovascular disorders (36, 37). The tracer methodology and computational modeling have been used to study the nonsteady-state kinetics of simpler metabolic networks, including plasma FFAs (38) and glucose metabolism (39). However, current modeling approaches fail in using isotope-labeled tracer data to accurately describe the dynamics of human lipoprotein metabolism under postprandial conditions without using unnatural feeding regimens, such as continuous feeding of small amounts during kinetics studies (40, 41). These methods can give valuable insights, but they do not reflect the natural eating habits of humans and they also do not comprehensively describe hepatic and intestinal lipoprotein dynamics.

Recently, a physiologically relevant computational model was developed to describe the nonsteady-state dynamics of the hepatic and intestinal lipoprotein metabolism on the basis of stable isotope–labeled tracer data collected during a mixed-meal test (42). Although this model provides valuable insights about the postprandial kinetics of hepatic and intestinal lipoproteins, it does not include a physiologically relevant gastrointestinal module. Furthermore, this model does not account for the postprandial effects of insulin on lipoprotein metabolism. Therefore, it cannot be used to investigate the effects of the anatomical changes caused by bariatric surgery and/or insulin-mediated processes on lipoprotein metabolism.

In the present study, we use a detailed, multicompartmental model of hepatic and intestinal lipoprotein metabolism to investigate the postprandial interactions between glucose and lipid pathways in patients with severe obesity and after bariatric surgery–induced weight loss. We recruited 24 patients and performed detailed postprandial lipoprotein kinetics experiments at baseline and at 1 year after RYGB. We also performed hyperinsulinemic-euglycemic clamps (HECs) to assess the interactions between lipoprotein and glucose–insulin kinetics. Taken together, our model provides deep insight into the postprandial lipoprotein metabolism of patients with severe obesity and into the changes induced by bariatric surgery.

Results

Patient characteristics. The study population comprised 24 patients with severe obesity (Table 1). At 1-year follow-up, RYGB resulted in significant weight loss in all patients. In addition, RYGB was associated with important improvements in metabolic health, including reduced intrahepatic TG (IHTG) content, plasma lipid concentrations, insulin sensitivity, and glycemia (Table 1).

Postprandial concentrations of VLDL$_1$ TG and apoB, and VLDL$_2$ TG are reduced after RYGB. All patients underwent a lipoprotein kinetics study that included a mixed-meal test at baseline and 1 year after the surgery. During the study, plasma VLDL$_1$ and VLDL$_2$ apoB (Figure 1, A and B), TG (Figure 1, C and D), CM TG (Figure 1E), and total plasma TG (Figure 1F) were measured up to 10 hours. At 2 hours, patients were asked to consume a mixed meal, and the postprandial phase started. In Figure 1, box plots show the presurgery (red) and postsurgery (blue) AUCs calculated for the postprandial state. One of the key differences between pre- and postsurgery apoB and TG profiles was the response to the mixed meal. Before surgery, meal ingestion was followed by pronounced VLDL$_1$ and VLDL$_2$ apoB (Figure 1, A and B, red) and TG (Figure 1, C and D, red) accumulation in the plasma. However, after the surgery, VLDL$_1$ and VLDL$_2$ apoB (Figure 1, A and B, blue) and TG (Figure 1, C and D, blue) concentrations were only moderately increased after the meal. After the surgery, the VLDL$_1$ apoB AUC was significantly reduced (Figure 1A), whereas VLDL$_2$ apoB AUC remained unchanged (Figure 1B). On the other hand, both VLDL$_1$ and VLDL$_2$ TG AUCs were significantly reduced after the surgery (Figure 1, C and D). The average TG to apoB ratio, which is calculated as the ratio of the TG to apoB AUCs, did not change in the VLDL$_1$ fraction (31.1 ± 7.1 vs. 28.8 ± 8.2 mg TG/mg apoB), but it was reduced in the VLDL$_2$ fraction (8.7 ± 2.3 vs. 6.3 ± 1.9 mg TG/mg apoB; $P < 0.001$) after the surgery. This indicates a decline in average VLDL$_2$ particle size after the surgery. The CM TG AUC (Figure 1E) and plasma TG AUC (Figure 1F) were also significantly reduced after the surgery. Our modeling results show that postsurgery reduction in the postprandial CM TG concentration resulted from reduced lipid absorption from intestine and enhanced CM TG clearance rate. After the surgery, the estimated CM TG clearance rate was increased by 72% on average ($P < 0.001$).

Figure 1 also shows that after the surgery, postprandial plasma VLDL apoB and TG exhibit faster dynamics. After the surgery, plasma VLDL$_1$ and VLDL$_2$ apoB and TG levels peaked earlier, compared with presurgery. After the surgery, postprandial plasma VLDL$_1$ apoB peak time was decreased from 4.8 ± 1.5 to 3.3 ± 0.7 hours ($P < 0.0005$), and plasma VLDL$_2$ apoB peak time was reduced from 6.0 ± 1.6 to 4.1 ± 1.2 hours ($P < 0.0001$). Similar peak-time reductions were observed for plasma VLDL$_1$ TG (4.8 ± 1.5 vs. 3.3 ± 0.6 hours; $P < 0.0005$) and VLDL$_2$ TG (5.7 ± 1.6 vs. 3.7 ± 0.8 hours; $P < 0.0001$) after the surgery. Moreover, postsurgery plasma VLDL$_1$ and VLDL$_2$ apoB and TG concentrations returned to their respective baselines within the observation time frame; this was not the case before the surgery.

A similar pattern was evident for CM TG and plasma TG time courses. Before the surgery, meal intake was followed by a significant increase in CM TG (Figure 1E, red) and plasma TG (Figure 1F, red) concentrations. After the surgery, postprandial CM TG and plasma TG elevations were lower as compared with presurgery status (Figure 1, E and F, blue). Our results show that after the surgery, CM TG peak time does not change much (4.9 ± 0.4 vs. 4.6 ± 0.6 h). The lack of reduction in CM TG peak time may be due, in part, to the slower meal consumption after the surgery (10 vs. 30 minutes; see Methods and Supplemental Methods for details). However, total plasma TG peak time is reduced after the surgery (5.9 ± 0.9 vs. 5.1 ± 0.8 h; $P < 0.01$). After surgery, CM TG and plasma TG levels also returned to their baselines within the observation time frame (Figure 1, E and F, blue).

RYGB is associated with reduced postprandial VLDL$_1$ TG and apoB production and increased postprandial VLDL$_2$ TG clearance. To gain more insight into the mechanisms underlying the observed changes in lipoprotein kinetics, isotopic enrichment data from different pools were assessed and analyzed using the computational model described in Methods. In Figure 2, pre- and postsurgery isotopic enrichment data from VLDL$_1$ and VLDL$_2$ apoB (Figure 2, A and B) and TG (Figure 2, C and D) pools, as well as plasma leucine (Figure 2E) and glycerol (Figure 2F) pools, are shown along with the model simulations. The results in Figures 1 and 2 show that the dynamics of the plasma concentrations and enriched materials in different pools are accurately captured by the computational model, allowing the calculation of the parameters that describe VLDL$_1$ and VLDL$_2$ apoB and TG kinetics in detail. Pre- and postsurgery kinetic parameters were estimated for each patient, and their averages are given in Table 2.

After the surgery, VLDL$_1$ apoB production rate was decreased (Table 2), whereas VLDL$_2$ apoB direct production rate, which is the rate at which apoB is directly secreted in the form of VLDL$_2$ from liver, did not change. As a consequence, the relative fraction of apoB that was directly secreted as VLDL$_2$ from liver

Table 1. Clinical and biochemical characteristics of included patients (N = 24) before and after surgery

Parameter	Before surgery	After surgery	P values
Sex (female; male), no.	12;12		
Age (years)	46.1 ± 11	47.1 ± 11	
Weight (kg)	135.1 ± 23.4	98.6 ± 18.6	<0.005
Body fat content (%)	45.6 ± 5.9	30.9 ± 10.6	<0.005
FFM (kg)	73.3 ± 14.8	66.6 ± 12.9	<0.01
Excess weight (kg)	57.8 ±20.0	21.3 ± 16.6	<0.005
BMI (kg/m^2)	43.4 ± 6	31.7 ± 5.1	<0.005
IHTG content (%)	9.9 ± 9.0	4.0 ± 1.7	<0.01
Plasma cholesterol (mmol/L)	4.9 ± 0.8	4.1 ± 0.6	<0.005
HDL cholesterol (mmol/L)	1.2 ± 0.2	1.5 ± 0.3	<0.005
LDL cholesterol (mmol/L)	3.1 ± 0.7	2.2 ± 0.6	<0.005
Plasma TG (mmol/L)	1.3 ± 0.6	0.8 ± 0.5	<0.005
apoB (mg/dL)	81.5 ± 16.6	67.1 ± 19.7	<0.005
Fasting FFA (mmol/L)	0.66 ± 0.18	0.63 ± 0.14	0.25
Fasting glucose (mmol/L)	5.0 ± 0.6	4.5 ± 0.3	<0.005
Fasting insulin (pmol/L)	143.2 ± 77.1	41.5 ± 23.7	<0.005
HOMA-IR	4.4 ± 2.5	1.2 ± 0.7	<0.005
Basal EGP (μmol/kg FFM/min)	12.6 ± 1.5	12.2 ± 1.9	0.5
Basal lipolysis (μmol/kg/min)	2.5 ± 0.8	3.8 ± 1.7	<0.01
Insulin suppression of EGP during step 1 of clamp (% of basal)	75.2 ± 14.0	93.1 ± 17.5	<0.01
Insulin suppression of lipolysis during step 1 of clamp (% of basal)	52.6 ± 20.2	80.3 ± 9.4	<0.005
Insulin stimulation of R$_d$ during step 2 of clamp (% of basal)	404.5 ± 156.5	544.2 ± 111.7	<0.005

Data are given as mean ± SD. Paired-sample t test was used to test the statistical significance of the differences between pre- and postsurgery values. FFM, fat-free mass.

was increased from 32% ± 14% to 43% ± 16% (P <0.05) after the surgery. On the other hand, the fractional transfer rate (FTR) of apoB from the VLDL$_1$ pool to the VLDL$_2$ pool tended to increase. Consequently, the total VLDL$_2$ apoB production rate, which is the sum of the VLDL$_2$ apoB that is directly secreted from liver and the VLDL$_2$ apoB that is derived from the VLDL$_1$ pool in circulation, is slightly increased, but this change did not reach statistical significance. The VLDL$_1$ TG production rate was significantly reduced, as was the VLDL$_2$ TG direct production rate. These findings indicate a noticeable shift in the distribution of hepatic TG secretion toward VLDL$_2$ (18% ± 12% vs. 23% ± 11%; P < 0.1) after the surgery. Together with the increase observed in the VLDL$_1$ TG FTR, the total VLDL$_2$ TG production rate remained the same after surgery.

After surgery, the VLDL$_1$ apoB fractional catabolic rate (FCR) did not change (Table 2), whereas the VLDL$_2$ apoB FCR tended to increase. In line, the VLDL$_1$ apoB fractional direct catabolic rate (FDC), which is the rate at which VLDL$_1$ apoB is directly removed from the circulation, did not change. After the surgery, a remarkable increase took place in VLDL TG catabolic rates, whereby VLDL$_1$ TG FCR tended to increase from 27.7 ± 23.4 to 34.0 ± 17.0 pools/d (P = 0.1) and VLDL$_2$ TG FCR was significantly increased from 10.8 ± 6.1 to 17.0 ± 10.1 pools/d (P = 0.002). However, the VLDL$_1$ TG FDC did not change after surgery.

Insulin-mediated stimulation of lipoprotein lipolysis is enhanced after surgery. After surgery, the homeostatic model assessment of insulin resistance (HOMA-IR) was significantly reduced (4.4 ± 2.5 vs. 1.2 ± 0.7; P < 0.005), and it was positively related to VLDL$_1$ apoB and TG production. After the surgery, there was a significant positive correlation between HOMA-IR and VLDL$_1$ apoB (r = 0.61; P < 0.005; Figure 3A, blue) and TG (r = 0.65; P <0.005; Figure 3B, blue) production rates. In the presurgery condition, trends between VLDL$_1$ apoB and TG production and HOMA-IR were the same, but the correlations were not statistically significant. When pre- and postsurgery data were combined and analyzed together, the correlations between HOMA-IR and VLDL$_1$ apoB production (r = 0.39; P < 0.01; Figure 3A, black) and VLDL$_1$ TG production (r = 0.53; P < 0.005; Figure 3B, black) remained significant. On the other hand, VLDL$_2$ apoB or TG production was not correlated with HOMA-IR before or after surgery.
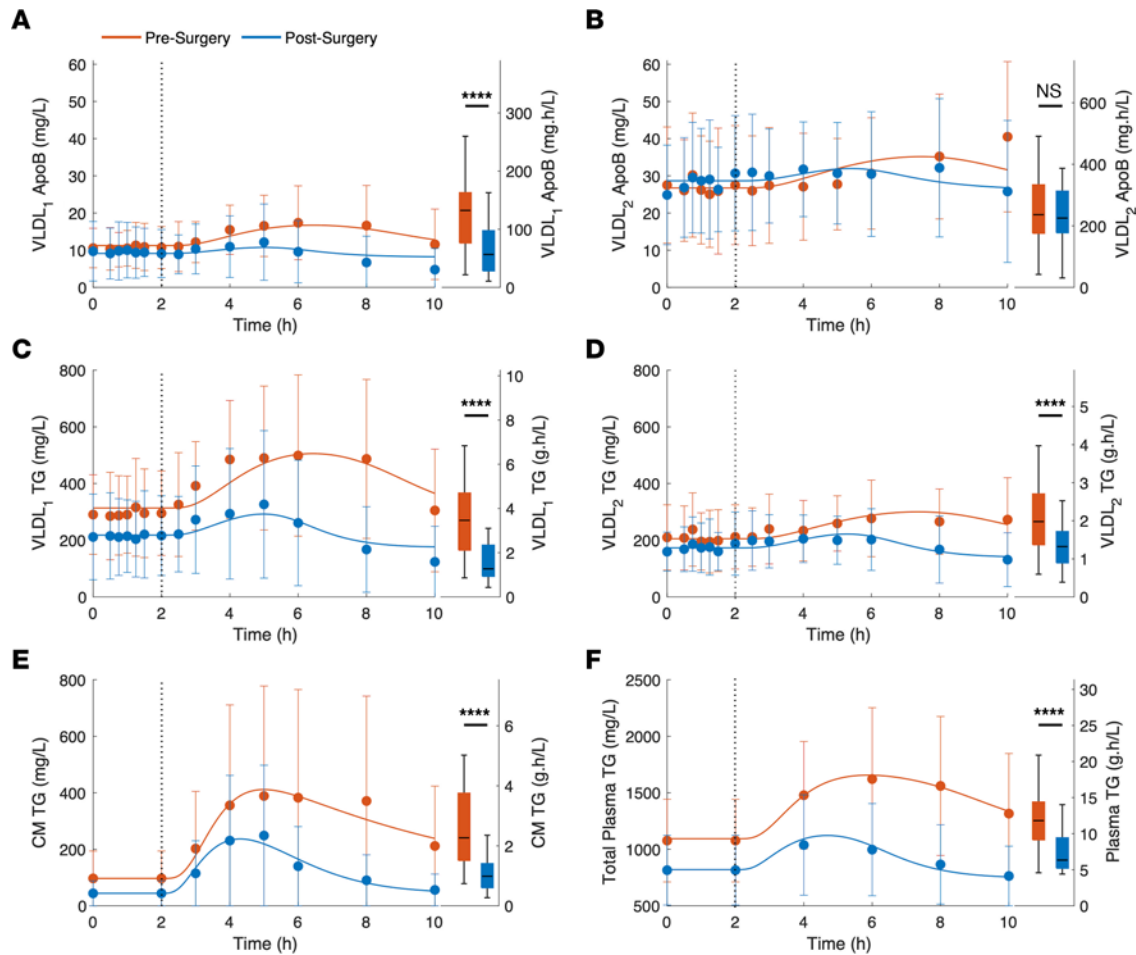
Figure 1. Plasma apoB and TG concentration time courses. (**A**–**F**) Presurgery (red) and postsurgery (blue) plasma $VLDL_1$ and $VLDL_2$ apoB (**A** and **B**), TG (**C** and **D**), plasma CM TG (**E**), and plasma TG (**F**) concentrations measured during the lipoprotein kinetics studies. Filled circles and error bars show data as mean ± SD. Solid curves show model simulations generated with model parameters estimated from average data (Supplemental Table 2). Dotted vertical lines mark mixed-meal ingestion time points. The box plots show the presurgery (red) and postsurgery (blue) AUCs calculated for the postprandial state (2–10 hours). Statistical significance was tested with a paired-sample t test. ****$P < 0.0005$.

Because insulin regulates both glucose and lipid homeostasis, we aimed to quantify the contribution of insulin to the regulation of postprandial lipoprotein metabolism, by incorporating an insulin-mediated stimulation of lipoprotein lipolysis pathway into the computational model. The responsiveness of the lipoprotein lipolysis pathway to circulating insulin can be expressed as the lipoprotein lipolysis insulin sensitivity index (ISI), which was estimated by model from the individual patient experimental data as described in the Supplemental Methods. In 5 patients, the model detected no insulin effect on lipoprotein lipolysis before surgery, but there was a detectable effect at 1-year follow-up. In all patients, the postsurgery lipoprotein lipolysis ISI was significantly increased (0.2 ± 0.15 vs. 0.42 ± 0.21; $P < 0.001$; Figure 4A). Furthermore, parameters of insulin sensitivity from the clamp studies were directly correlated to the model-derived lipolysis ISI in patients after surgery (Figure 4, B–D).

Discussion

Data from this study demonstrate that bariatric surgery is not only associated with significant weight loss and improved metabolic health but also with decreased postprandial $VLDL_1$ production, increased postprandial $VLDL_2$ clearance, and improved insulin sensitivity of the lipolysis pathway. Using physiology-based kinetic modeling, we provide deeper insight into the complexity of human lipoprotein homeostasis. We show that the reduction in plasma VLDL apoB after bariatric surgery is a consequence of seemingly opposing effects on $VLDL_1$ versus $VLDL_2$ apoB kinetics: $VLDL_1$ apoB production was reduced, with an unaltered $VLDL_1$ apoB catabolic rate, whereas the $VLDL_2$ apoB direct production rate was unaltered, but its clearance rate tended to
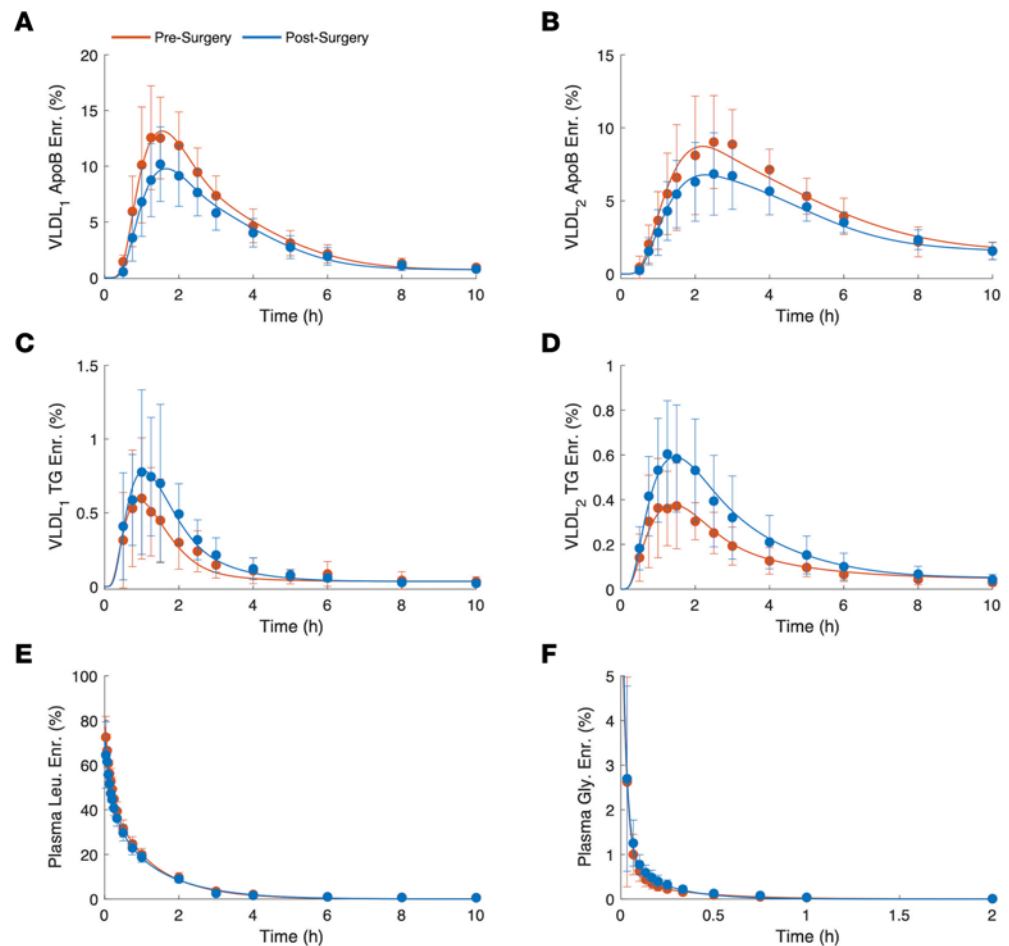
Figure 2. Leucine and glycerol enrichment time-courses. Presurgery (red) and postsurgery (blue) population averages for enrichment data (filled circles with error bars) and the model simulations (solid lines). (**A** and **B**) $VLDL_1$ and $VLDL_2$ apoB [5,5,5-$^2H_3$]-leucine (Leu.) enrichments (Enr.). (**C** and **D**) $VLDL_1$ and $VLDL_2$ TG [1,1,2,3,3-$^2H_5$]-glycerol (Gly.) enrichments. (**E**) Plasma [5,5,5-$^2H_3$]-leucine enrichment. (**F**) Plasma [1,1,2,3,3-$^2H_5$]-glycerol enrichment. Data are presented as mean ± SD.

be increased. Together, these findings imply a shift from the hepatic secretion of large $VLDL_1$ particles before surgery toward the secretion of smaller $VLDL_2$ particles after surgery. Consistent with such a shift, we found that the relative fraction of hepatic apoB that was secreted in the form of $VLDL_2$ increased by more than 33% after surgery. Moreover, bariatric surgery–induced weight loss was associated with decreased VLDL TG concentrations in both fractions, and our computational modeling indicated that this reduction was due to decreased $VLDL_1$ TG production as well as increased $VLDL_1$ and $VLDL_2$ TG turnover.

Previously, Padilla et al. (41) studied the impact of gastric bypass and sleeve gastrectomy on hepatic apoB kinetics under constant feeding conditions. They reported a significant decrease in plasma VLDL apoB after both gastric bypass and sleeve gastrectomy surgeries, due to reduced hepatic production and increased fractional catabolic rate. For the gastric bypass, their report showed a trend toward a decrease in hepatic apoB production, but the apoB fractional catabolic rate remained the same (41). However, their study did not account for the different VLDL subfractions and, more importantly, their data were collected under a constant feeding regimen, which does not reflect natural eating habits. Several other studies investigated postprandial plasma lipid profiles after bariatric surgery. In patients with obesity and/or type 2 diabetes, it was shown that postprandial plasma TG and plasma cholesterol concentrations were significantly reduced during a mixed-meal test that was performed 2 weeks after the sleeve gastrectomy or gastric bypass (43). In a follow-up study, similar postprandial reductions in plasma TG and cholesterol concentrations were reported 2 years after the surgery (44). In a third study, a standard oral fat-load test was performed 3 months after sleeve gastrectomy, and a significant reduction in postprandial VLDL CM-remnant TG concentration was reported (45). Although, the reported postsurgery changes in plasma TG concentrations in

Table 2. Pre- and postsurgery kinetic parameters

Parameter	Before surgery	After surgery	P values
VLDL$_1$ apoB production rate (mg/d)	867.9 ± 510	667.9 ± 624.2	0.05
VLDL$_1$ apoB FTR (pools/d)	6.2 ± 7.8	8.2 ± 7.7	0.16
VLDL$_1$ apoB FCR (pools/d)	18.0 ± 11.6	21.1 ± 13.1	0.14
VLDL$_1$ apoB FDC (pools/d)	11.9 ± 5.7	13.0 ± 6.8	0.19
VLDL$_1$ TG production rate (g/d)	34.2 ± 18.2	23.4 ± 15.2	0.005
VLDL$_1$ TG FTR (pools/d)	2.8 ± 2.5	5.4 ± 6.3	0.02
VLDL$_1$ TG FCR (pools/d)	27.7 ± 23.4	34.0 ± 17.0	0.10
VLDL$_1$ TG FDC (pools/d)	24.9 ± 21.8	28.6 ± 12.6	0.20
VLDL$_2$ apoB direct production rate (mg/d)	404.7 ± 254.8	409.7 ± 315.2	0.46
VLDL$_2$ apoB total production rate (mg/d)	611.3 ± 328.2	647.6 ± 439.3	0.31
VLDL$_2$ apoB FCR (pools/d)	5.4 ± 2.9	6.7 ± 4.1	0.06
VLDL$_2$ TG direct production rate (g/d)	7.5 ± 8.2	6.5.3 ± 4.4	0.31
VLDL$_2$ TG total production rate (g/d)	10.6 ± 8.9	10.5 ± 7.3	0.49
VLDL$_2$ TG FCR (pools/d)	10.8 ± 6.1	17.0 ± 10.1	0.002

VLDL$_1$ and VLDL$_2$ apoB and TG kinetics before and after surgery. Data are presented as mean ± SD; statistical significance is tested by paired-sample t test.

these studies are consistent with our findings, the design of these studies did not allow the researchers to investigate the production or the turnover kinetics of lipoproteins. Hence, they could not provide mechanistic insights of reduced plasma concentrations.

An advantage of our computational modeling–based approach was that the detailed insight could be obtained in pre- and postsurgery dynamic regulation of lipoprotein metabolism during the postprandial state. Our data show that in the presurgery phase, there is a profound VLDL accumulation in plasma during the postprandial state. In line with earlier reports, we hypothesize that this is primarily due to the competition for LPL-mediated lipoprotein lipolysis (46–50). The competition between different lipoprotein species for lipolysis pathways becomes particularly evident in the postprandial state as the digested lipids enter the circulation in the form of CMs. Studies show a positive relation between particle size and the lipolysis rate (51–53), which gives CMs the priority for lipolysis by LPL. Hence, in the postprandial state, increased CM size in the circulation promotes competition and results in a significant reduction in VLDL apoB and TG FCRs and FTRs. Our results show that, after surgery, postprandial plasma VLDL apoB and TG concentrations do not increase much (Figure 1, blue), compared with the presurgery condition (Figure 1, red), for 3 reasons. First, after surgery, hepatic apoB and TG production are significantly reduced. Second, reduced postsurgery intestinal lipid absorption and increased CM TG clearance rate result in lower plasma CM TG (Figure 1E, blue). Although, reduced intestinal lipid absorption is a model estimate and has not been verified by measuring lipids in stool samples, it is consistent with previous studies showing a significant reduction in intestinal lipid absorption after RYGB surgery (54–58). Hence, in the postprandial state, the competition between hepatic and intestinal lipoproteins for the lipolysis pathways remains weak. Third, after surgery, postprandial stimulation of lipoprotein lipolysis by insulin is greatly improved (Figure 4A). As a consequence of these factors, after surgery, postprandial VLDL apoB and TG accumulation in plasma remains modest. Furthermore, elevated plasma TG and apoB concentrations return to their baselines within the time course of the study (8 hours), whereas postprandial lipids remain elevated for more than 8 hours, on average, in the presurgery condition. This implies that, after surgery, after consuming a meal, the plasma lipid profiles are more likely to return to their baselines before the next meal is consumed and this effectively prevents residual lipids from the previous meal to further increase plasma lipid concentrations.

In this study, we also demonstrated significant improvements in postsurgery insulin-responsiveness indices, and a positive correlation between insulin resistance and hepatic VLDL$_1$ production after the surgery. Insulin reduces hepatic VLDL secretion by reducing apoB lipidation and promoting apoB degradation in the hepatocyte (59–61). The HOMA-IR index was significantly reduced after surgery. We showed that HOMA-IR was positively correlated with postsurgery VLDL$_1$ TG and apoB production (Figure 3, A and B) but not with VLDL$_2$ apoB or TG production. This finding emphasizes the role that insulin plays in the regulation of hepatic lipoprotein production, whereby patients with high insulin resistance tend to produce greater
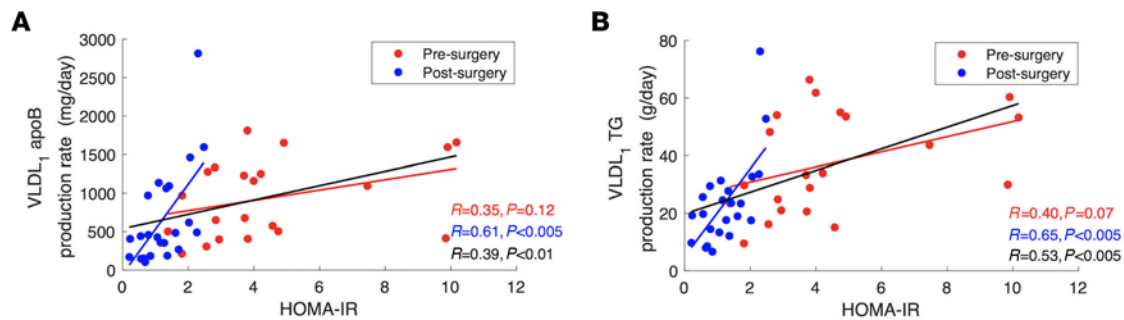
Figure 3. Relationship between pre- and postsurgery VLDL₁ apoB and TG production rates and HOMA-IR. (A and B) The regression lines for pre- and postsurgery data and combined data are shown in red, blue, and black, respectively. Correlation coefficients (r) and associated P values are reported in each panel.

amounts of large hepatic lipoproteins. The lack of association between VLDL$_2$ apoB or TG production and HOMA-IR might be explained by independent regulation of hepatic VLDL$_1$ and VLDL$_2$ apoB production, as suggested before (10, 11). This indicates that the production of larger hepatic lipoprotein particles is increased with insulin resistance, but the production of smaller lipoprotein particles is not affected. The lack of a statistically significant association between presurgery insulin resistance indices and estimated kinetic parameters might be due to the relatively high insulin resistance and large interpatient variability in comparison with the relatively small population size. Nevertheless, when pre- and postsurgery data were analyzed together, the correlations between HOMA-IR and VLDL$_1$ apoB and TG production (Figure 3, A and B, black) remained significant. This may indicate that, after surgery, the associations between HOMA-IR and VLDL$_1$ apoB and TG production do not change but become more pronounced.

We also show in this study a postsurgery improvement in insulin-mediated stimulation of the lipoprotein lipolysis pathway. Insulin is known to stimulate lipoprotein lipolysis by its impact on LPL at both the transcriptional and posttranslational levels (62, 63). To quantify the responsiveness of the lipoprotein lipolysis pathway to circulating insulin, we have introduced the lipoprotein lipolysis ISI, which was estimated for each patient by using individual experimental data with the model. Our results, indeed, show that insulin-mediated stimulation of lipoprotein lipolysis was improved after the surgery, as reflected in the significantly increased lipoprotein lipolysis ISI (0.20 ± 0.15 vs. 0.42 ± 0.20; $P < 0.001$; Figure 4A). Moreover, calculated postsurgery lipoprotein lipolysis ISI values were strongly correlated with measured insulin-mediated adipose tissue lipolysis suppression (Figure 4B), endogenous glucose production (EGP) suppression (Figure 4C), and glucose disposal rate (R_d) stimulation (Figure 4D) indices. because the lipoprotein lipolysis ISI is defined as the sensitivity of the lipoprotein lipolysis pathway to the fractional increase in insulin over the baseline, we compared lipoprotein lipolysis ISI with the clamp-derived sensitivity indices normalized over the fractional increase in insulin during the clamp studies. However, the associations between lipoprotein lipolysis ISI and clamp-derived insulin sensitivity parameters were not present for presurgery data (Supplemental Figure 5; supplemental material available online with this article; https://doi.org/10.1172/jci.insight.166905DS1). This may be due, in part, to the fact that model could not detect an insulin-mediated lipoprotein lipolysis stimulation in the data of 5 of the 24 patients before surgery. Nevertheless, a linear trend between lipoprotein lipolysis ISI and insulin-mediated lipolysis suppression was evident in the combined pre- and postsurgery data (Supplemental Figure 5B), which was not the case for other clamp-derived insulin-sensitivity parameters (Supplemental Figure 5, C and D). The dynamics of the insulin-mediated suppression of the hepatic apoB production was also incorporated into the model as a delayed forcing signal generated by the portal vein insulin; the portal vein insulin signal was derived from plasma insulin data. However, insulin-mediated effects on the hepatic apoB production pathway remained undetectable due to the uncertainty associated with portal vein insulin concentration and resulting parameter estimates. Therefore, insulin-mediated suppression of the hepatic apoB production was removed from the final version of the model.

Glucagon-like peptide-1 (GLP-1) is best known for its role in glucose homeostasis and insulinotropic effects (64–66). However, GLP-1 also plays a direct role in lipid and lipoprotein metabolism (67), and thus the GLP-1 receptor pathway has been the focus of pharmacological lipid research (68). GLP-1 reduces intestinal CM production and secretion (69, 70), and activation of GLP-1 receptors reduces hepatic VLDL production (71, 72). Moreover, GLP-1 also triggers a signal through the intrinsic gut–liver axis and
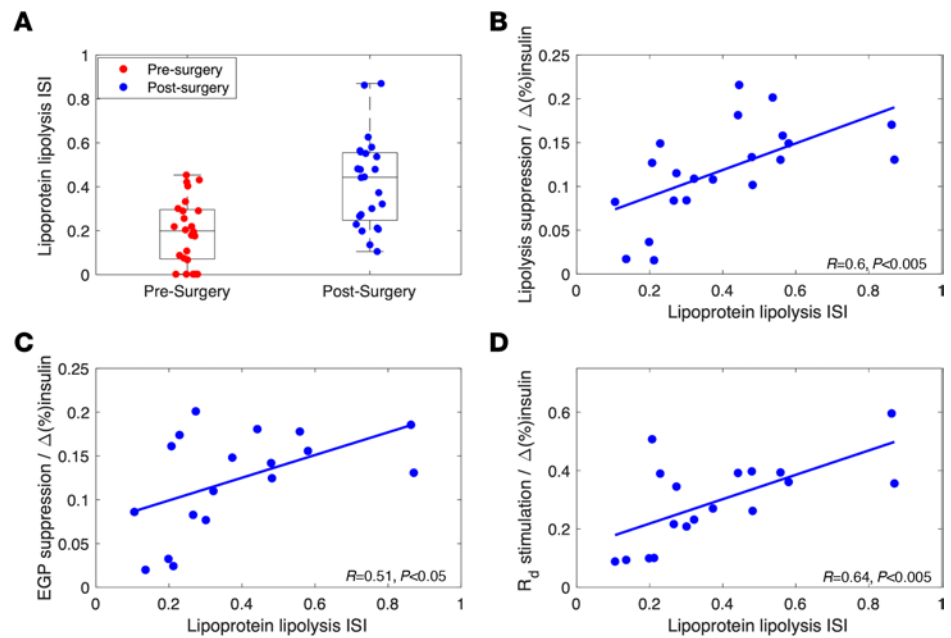
Figure 4. Relationship between lipoprotein lipolysis ISI and tissue specific insulin responsiveness indices. (**A**) Pre- and postsurgery lipoprotein lipolysis ISI. (**B**) Postsurgery insulin-mediated peripheral lipolysis suppression per insulin increased over basal level (Δ[%]insulin) from the clamp studies vs lipoprotein lipolysis ISI. (**C**) Postsurgery insulin-mediated EGP suppression per Δ(%)insulin versus lipoprotein lipolysis ISI. (**D**) Postsurgery insulin-mediated R_d stimulation per Δ(%)insulin versus lipolysis ISI. In each panel, the regression lines for the postsurgery data are shown in blue. Correlation coefficients (r) and associated P values are reported in each panel.

ameliorates diet-induced hepatic VLDL overproduction (73). These studies suggest that, other than being a potent insulin secretagogue, GLP-1 regulates lipoprotein metabolism in an insulin-independent manner. Our results show that, after RYGB surgery, fasting GLP-1 levels do not change (3.5 ± 3.9 vs. 4.1 ± 3.6 pmol/L; $P = 0.26$; Supplemental Figure 4). However, postprandial GLP-1 levels are significantly increased (AUC: 2139.2 ± 1093.5 vs. 7204.3 ± 4106.4 pmol/min/L; $P < 0.005$; Supplemental Figure 4), which is consistent with earlier reports showing a significant increase in GLP-1 levels after RYGB surgery (74–79). It is suggested that elevated GLP-1 levels play an important role in several metabolic improvements and diabetes remission after RYGB surgery (27, 78–81). Thus, postsurgery reduction in VLDL production and improved insulin-mediated processes may be, in part, a consequence of elevated GLP-1 levels.

TG homeostasis directly influences hepatic steatosis, for which our data indicate a significant reduction in IHTG after surgery (9.9% ± 9.0% vs. 4.0% ± 1.7%; $P < 0.05$) as reported before (82–84). Adiels et al. (10) proposed that increased hepatic fat content as a consequence of increased FFA flux to the liver due to insulin resistance results in overproduction of larger VLDL$_1$ particles. However, it is not clear whether this association was a direct impact of hepatic insulin resistance or increased IHTG that was secondary to insulin resistance, because insulin resistance and hepatic steatosis are common comorbidities (85, 86). Indeed, we showed a strong association between postsurgery HOMA-IR and VLDL$_1$ apoB and TG production but not VLDL$_2$, which is consistent with earlier reports (10, 11).

We used a physiologically based, large computational model and a comprehensive data set to investigate the impact of RYGB surgery on VLDL$_1$ and VLDL$_2$ apoB and TG kinetics under the nonsteady-state postprandial condition during a mixed-meal test. The study was designed to capture dynamic responses to natural eating regimens as closely as possible. The complex and dynamic nature of lipoprotein metabolism, together with multiple interactions occurring postprandially, made it necessary to make assumptions and simplifications during the model development. We acknowledge that like all models that have been proposed in the literature and all the models that will follow, our model is not a complete account of the entire physiological processes involved. The developed model is not intended to capture all the biochemical or molecular details of the lipoprotein metabolism. The computational model was developed in a way to extract as much information as possible from the available data while preserving physiological relevance.

Conclusion. We conclude that physiologically based mathematical modeling of postprandial apoB and TG metabolism in different VLDL fractions in combination with gold standard measurements of insulin sensitivity provide deep insight into the effects of RYGB surgery on lipid handling and its interaction with glucose metabolism and insulin in the postprandial state. RYGB restores the homeostatic balance between insulin sensitivity and TG production and catabolism. Taken together, our experimental data, combined with computational modeling, show that RYGB in morbidly obese patients results in reduced postprandial VLDL TG due to reduced $VLDL_1$ production and increased $VLDL_2$ TG clearance rates, with improved responsiveness of lipoprotein homeostasis to circulating insulin levels.

Methods

Design. This multicenter, observational intervention study was part of RESOLVE (A systems biology approach to RESOLVE the molecular pathology of two hallmarks of patients with metabolic syndrome and its comorbidities; hypertriglyceridemia and low HDL-cholesterol), a European research program on the metabolic syndrome. We designed the present study to evaluate postprandial lipoprotein kinetics in humans before and after bariatric surgery–induced weight loss and their relation to insulin-mediated processes. For this purpose, we developed a physiologically based computational model of human lipoprotein metabolism and used this model to analyze in vivo data collected during the baseline (before surgery) and 1 year after the RYGB.

Study population. We recruited patients with severe obesity from the outpatient clinic of 2 obesity centers in the Amsterdam metropolitan area. Patients were eligible to participate in the present study if they (a) were older than 18 years; (b) met criteria for bariatric surgery in accordance with national guidelines (87); (c) were scheduled for elective RYGB; and (d) had stable weight for at least 3 months before surgery. Exclusion criteria were (a) the use of alcohol (>2 units/d) or recreational drugs; (b) the use of lipid-lowering drugs, exogenous insulin, incretin mimetics, or psychoactive medication; (c) chilDVHood-onset obesity; or (d) any somatic disorder except for common obesity-related conditions (e.g., dyslipidemia, hypertension, obstructive sleep apnea).

Lipoprotein kinetics studies. Lipoprotein kinetics experiments were performed using $[5,5,5-^2H_3]$-leucine and $[1,1,2,3,3-^2H_5]$-glycerol to determine in vivo apoB and TG fluxes in $VLDL_1$ and $VLDL_2$ fractions (Supplemental Figure 1A). Experiments were performed shortly (<4 weeks) prior to the scheduled RYGB surgery and repeated 1 year after the operation. After an overnight fast, $[5,5,5-^2H_3]$-leucine (7 mg/kg BW; 99% enriched; Cambridge Isotopes) and $[1,1,2,3,3-^2H_5]$-glycerol (500 mg; >99% enriched; Cambridge Isotopes) were infused via a venous catheter. Two hours after tracer infusion, patients received a liquid mixed meal that consisted of 2 bottles of Fresubin Protein Energy (Fresenius Kabi), 40 mL of olive oil, 2 g of cacao powder, and 5 tablets of a noncaloric sweetener (Hermesetas; Hermes Sweeteners) (Supplemental Table 1). Patients were instructed to consume the meal within 10 minutes before surgery or within 30 minutes at 1-year follow-up. After the surgery, patients were given more time to consume the meal because they experienced difficulty in completing the meal within 10 minutes. At 5, 15, 30, 45, 60, 75, 90, 120, 150, 180, 240, 300, 360, 480, 600, and 1440 minutes after infusion, venous blood samples were drawn for the determination of $[5,5,5-^2H_3]$-leucine and $[1,1,2,3,3-^2H_5]$-glycerol enrichment in plasma and lipoprotein fractions.

Isolation of VLDL subfractions. $VLDL_1$ and $VLDL_2$ fractions were isolated from plasma by 3-step gradient ultracentrifugation using a SW41 rotor (Beckman) in an Optima XPN-100 Beckman ultracentrifuge. In short, the density (d) of 4 mL of plasma was adjusted to 1.1502 g/mL with NaCl. Then 0.5 mL of NaBr/NaCl (d = 1.182 g/mL) and 4 mL of plasma (d = 1.1502 g/mL) was transferred to an ultraclear Beckman SW41 tube. The gradient was formed by layering 2 mL of salt solutions of the following densities on the top of the plasma: (a) 1.079 g/mL; (b) 1.0722 g/mL; (c) 1.0641 g/mL; and (d) 1.0588 g/mL. The different fractions were isolated using the following conditions: for CMs (d < 1.006 g/mL): 30 minutes, 260,639 g; for $VLDL_1$: 51 minutes, 260,639 g; and for $VLDL_2$: 16.36 hours, 55,521 g. At each step, the upper 1 mL was aspirated and replaced by the appropriate density fraction. Isolated lipoprotein fractions were frozen at –80 °C until further analysis.

Determination of isotopic enrichments. To determine leucine enrichment in apoB, $VLDL_1$ and $VLDL_2$ fractions were precipitated with isopropanol, delipidated with ethanol-diethyl ether, dried, and hydrolyzed with 6M HCl at 110°C for 24 hours. The samples were then prepared for analysis of leucine enrichment as described (88, 89). Briefly, leucine enrichment was determined on a gas chromatography–mass spectrometry (GC-MS) (GC-MSD5975c; Agilent Technologies) equipped with a VF17ms column operated in selected ion monitoring mode, using norleucine as an internal standard. To calculate isotope enrichments, the average value of the *m/z*

161:158 ratio was determined using a calibration curve with known quantities of labeled and unlabeled leucine (90). The resulting m/z 161:158 was expressed as molar percent excess.

To determine glycerol enrichment in TG within $VLDL_1$ and $VLDL_2$, the isolated fractions were precipitated with isopropanol, delipidated with alcohol/diethyl ether, and solubilized in isopropanol. The phospholipids were removed by adding 2 g of activated zeolite (Merck) to each tube. After centrifugation, the samples were evaporated under N_2 at 80°C. Isopropanol was added and the samples were transferred to a 1.5 mL vial. The glycerol extracts were saponified with 2% KOH in ethanol, incubated for 2 hours at 60°C, and dried under N_2. Heptafluorobutyric acid (Sigma-Aldrich) and ethyl acetate, at a 1:3 ratio, and standards and controls were added and incubated for 10 minutes at 70°C. After evaporation under N_2, the samples were solved in ethyl acetate and analyzed by GC-MS as described before (89).

HEC. We determined basal and insulin-mediated glucose fluxes as well as lipolysis rates during a 2-step HEC using [6,6-^{2}H$_2$]-glucose and [1,1,2,3,3-^{2}H$_5$]-glycerol (Supplemental Figure 1B), as described elsewhere (91, 92). Briefly, primed continuous infusions of [6,6-^{2}H$_2$]-glucose (prime: 11 μmol/kg; continuous: 0.11 μmol/kg/min; >99% enriched; Cambridge Isotopes) and [1,1,2,3,3-^{2}H$_5$]-glycerol (prime: 1.6 μmol/kg; continuous: 0.11 μmol/kg/min; >99% enriched; Cambridge Isotopes) were started and continued until the end of the study. Basal glucose (EGP) and glycerol (from lipolysis) production were determined after 2 hours of tracer equilibration. Next, insulin-mediated suppression of EGP and insulin-mediated suppression of lipolysis were determined after 2 hours of low-dose insulin infusion (step 1: Actrapid 20 mU/m^2 body surface area/min; Novo Nordisk Farma). Finally, insulin-stimulated R_d was determined after an additional 2 hours of high-dose insulin infusion (step 2: 60 mU/m^2/min). During insulin infusion, blood glucose concentration was held at 5 mmol/L by frequent bedside monitoring and variable exogenous glucose infusion (enriched with 1% [6,6-^{2}H$_2$]-glucose to maintain stable enrichment in the plasma pool).

Biochemical analyses. Plasma glucose concentrations were determined with the glucose-oxidation method using a Biosen C-Line glucose analyzer (EFK Diagnostics). Insulin and cortisol were determined by immunoassay on an Immulite 2000 system (Diagnostic Products) with intra-assay variations of 4–5% and 3–6%, respectively. Glucagon was determined by radioimmunoassay (Linco Research) with an intra-assay variation of 4–8%. Plasma FFAs were analyzed by enzymatic colorimetric assay (NEFA-C kit, Wako Chemicals). Plasma total cholesterol, LDL cholesterol, HDL cholesterol, and TG were analyzed by a Selektra autoanalyzer (Sopachem). Plasma apoB was determined by immunoturbidimetric assay (Wako Chemicals) by a Selektra autoanalyzer.

Calculations of basal and insulin-mediated fluxes. We calculated glucose fluxes during HEC (EGP and the R_d) using modified versions of Steele equations for the steady state (basal fluxes) or nonsteady state (fluxes during the insulin infusion) (93, 94). Hepatic insulin sensitivity was defined as the percent suppression of EGP by step-1 hyperinsulinemia; peripheral or muscle insulin sensitivity was defined as the percent stimulation of glucose R_d by step-2 hyperinsulinemia (95). Basal whole-body lipolysis was defined as the glycerol rate of appearance, which, in turn, was determined using the tracer dilution method (96). Adipose tissue insulin sensitivity was defined as the percent suppression of lipolysis by step-1 hyperinsulinemia (97). Finally, given the interindividual variation in insulin clearance, parameters of insulin sensitivity were normalized to insulin levels during the clamp.

Determination of liver fat content and excess BW. IHTG was determined by proton magnetic resonance spectroscopy as described before (98). Excess weight was calculated as the weight that corresponds to the difference between the patient's BMI and a cutoff BMI value of 25 kg/m^2.

Computational modeling. We used a computational modeling approach to investigate the effects of the RYGB surgery on postprandial lipoprotein kinetics and to explore the complex interactions between glucose and lipid fluxes. To achieve this, we translated the metabolic network of systemic lipoprotein metabolism into a physiologically based mathematical model, as illustrated in Supplemental Figure 2. The model describes systemic lipoprotein kinetics using 5 interconnected modules: gastrointestinal, plasma, liver, tracer injection, and insulin. For computational simulations and analyses, the system dynamics were described with a system of ordinary differential equations. The mathematical model was then implemented into the MATLAB programming environment (MathWorks; R2018b). The kinetic transfer rate parameters were estimated from the experimental isotopic enrichment and biochemical concentration data, using MATLAB's optimization toolbox. The details of the computational model are given in Supplemental Methods.

Statistics. All statistical analyses were performed using the MATLAB programming environment. Normally distributed data are presented as mean ± SD. We used median and IQR to present nonnormally distributed data. We used 1-tailed, paired-sample t tests to compare baseline data with 1-year follow-up data. Bivariate correlations were evaluated using Pearson correlation coefficients. Findings were considered significant if $P < 0.05$.

Study approval. The study was approved by the Amsterdam University Medical Center Medical Ethics Committee. All participants provided written informed consent in accordance with the Declaration of Helsinki. The study was prospectively registered in the Netherlands Trial Registry (identifier NL4531; www.trialregister.nl).

Data availability. Computer codes for the computational model and data files are publicly available in the GitHub data repository at https://github.com/vehpi/lipoprotein_kinetics/tree/27f0e42919d-638e988a3a71d7cdb570e6cb20fdb. Additional information will be provided by the corresponding author upon request; values for all data points in graphs are reported in the Supporting Data Values file.

Author contributions

GMDT, NAWVR, MJS, AKG, and MN designed the study; KWTH, PWG, and MJS performed the human studies; DVH, HS, HJ, and AWMS performed the laboratory analysis; VY and NAWVR developed the computational model; VY wrote the computer programs, created figures and tables, and wrote the first draft; VY, KWTH, GMDT, NAWVR, MJS, AKG, and MN revised the first draft and finalized the manuscript.

Acknowledgments

Address correspondence to: Vehpi Yildirim, Department of Public and Occupational Health, Amsterdam University Medical Center, Meibergdreef 9, 1105 AZ Amsterdam, The Netherlands. Email: v.yildirim@amsterdamumc.nl.

1. Uzogara SG. Obesity epidemic, medical and quality of life consequences: a review. *Int J Public Heal Res*. 2017;5(1):1–12.
2. Klop B, et al. Dyslipidemia in obesity: mechanisms and potential targets. *Nutrients*. 2013;5(4):1218–1240.
3. Taskinen MR, et al. Dual metabolic defects are required to produce hypertriglyceridemia in obese subjects. *Arterioscler Thromb Vasc Biol*. 2011;31(9):2144–2150.
4. Ormazabal V, et al. Association between insulin resistance and the development of cardiovascular disease. *Cardiovasc Diabetol*. 2018;17(1):122.
5. Taskinen M-RR, Borén J. New insights into the pathophysiology of dyslipidemia in type 2 diabetes. *Atherosclerosis*. 2015;239(2):483–495.
6. Eckel RH, et al. Cardiovascular disease in diabetes, beyond glucose. *Cell Metab*. 2021;33(8):1519–1545.
7. Mittendorfer B, et al. VLDL triglyceride kinetics in lean, overweight, and obese men and women. *J Clin Endocrinol Metab*. 2016;101(11):4151–4160.
8. Avramoglu RK, et al. Lipid and lipoprotein dysregulation in insulin resistant states. *Clin Chim Acta*. 2006;368(1–2):1–19.
9. Adiels M, et al. Overproduction of very low-density lipoproteins is the hallmark of the dyslipidemia in the metabolic syndrome. *Arterioscler Thromb Vasc Biol*. 2008;28(7):1225–1236.
10. Adiels M, et al. Overproduction of large VLDL particles is driven by increased liver fat content in man. *Diabetologia*. 2006;49(4):755–765.
11. Gill JMR, et al. Hepatic production of VLDL1 but not VLDL2 is related to insulin resistance in normoglycaemic middle-aged subjects. *Atherosclerosis*. 2004;176(1):49–56.
12. Malmström R, et al. Effects of insulin and acipimox on VLDL1 and VLDL2 apolipoproteinB production in normal subjects. *Diabetes*. 1998;47(5):779–787.
13. Johansen RF, et al. Basal and insulin-regulated VLDL1 and VLDL2 kinetics in men with type 2 diabetes. *Diabetologia*. 2016;59(4):833–843.
14. Adiels M, et al. Acute suppression of VLDL1 secretion rate by insulin is associated with hepatic fat content and insulin resistance. *Diabetologia*. 2007;50(11):2356–2365.
15. Ference BA, et al. Low-density lipoproteins cause atherosclerotic cardiovascular disease. 1. Evidence from genetic, epidemiologic, and clinical studies. A consensus statement fromthe European Atherosclerosis Society Consensus Panel. *Eur Heart J*. 2017;38(32):2459–2472.
16. Brehm A, et al. Relationship between serum lipoprotein ratios and insulin resistance in obesity. *Clin Chem*. 2004;50(12):2316–2322.
17. Steinberger J, et al. Relationship between insulin resistance and abnormal lipid profile in obese adolescents. *J Pediatr*. 1995;126(5):690–695.
18. Sung KC, et al. Metabolic markers associated with insulin resistance predict type 2 diabetes in Koreans with normal blood pressure or prehypertension. *Cardiovasc Diabetol*. 2016;15(1):47.
19. van der Kolk BW, et al. Plasma lipid profiling of tissue-specific insulin resistance in human obesity. *Int J Obes*. 2019;43(5):989–998.
20. Petersen MC, Shulman GI. Mechanisms of insulin action and insulin resistance. *Physiol Rev*. 2018;98(4):2133–2223.
21. Wolfe BM, et al. Treatment of obesity: weight loss and bariatric surgery. *Circ Res*. 2016;118(11):1844–1855.

22. Peterli R, et al. Effect of laparoscopic sleeve gastrectomy vs laparoscopic roux-en-y gastric bypass onweight loss in patients with morbid obesity the sm-boss randomized clinical trial. *JAMA*. 2018;319(3):255–265.

23. Qi L, et al. Effects of bariatric surgery on glycemic and lipid metabolism, surgical complication and quality of life in adolescents with obesity: a systematic review and meta-analysis. *Surg Obes Relat Dis*. 2017;13(12):2037–2055.

24. Chondronikola M, et al. Bariatric surgery and type 2 diabetes: are there weight loss-independent therapeutic effects of upper gastrointestinal bypass? *J Intern Med*. 2016;280(5):476–486.

25. Buchwald H, Oien DM. Metabolic/bariatric surgery worldwide 2008. *Obes Surg*. 2009;19(12):1605–1611.

26. Peterli R, et al. Improvement in glucose metabolism after bariatric surgery: comparison of laparoscopic Roux-en-Y gastric bypass and laparoscopic sleeve gastrectomy: a prospective randomized trial. *Ann Surg*. 2009;250(2):234–241.

27. Umeda LM, et al. Early improvement in glycemic control after bariatric surgery and its relationships with insulin, GLP-1, and glucagon secretion in type 2 diabetic patients. *Obes Surg*. 2011;21(7):896–901.

28. Mulla CM, et al. Mechanisms of weight loss and improved metabolism following bariatric surgery. *Ann N Y Acad Sci*. 2018;1411(1):53–64.

29. Furet JP, et al. Differential adaptation of human gut microbiota to bariatric surgery-induced weight loss: links with metabolic and low-grade inflammation markers. *Diabetes*. 2010;59(12):3049–3057.

30. Fischer HP. Mathematical modeling of complex biological systems: from parts lists to understanding systems behavior. *Alcohol Res Health*. 2008;31(1):49–59.

31. Rozendaal YJW, et al. In vivo and in silico dynamics of the development of metabolic syndrome. *PLoS Comput Biol*. 2018;14(6):e1006145.

32. Packard CJ, et al. Development and application of a multicompartmental model to study very low density lipoprotein subfraction metabolism. *J Lipid Res*. 1995;36(1):172–187.

33. Adiels M, et al. A new combined multicompartmental model for apolipoproteinB-100 and triglyceride metabolism in VLDL subfractions. *J Lipid Res*. 2005;46(1):58–67.

34. Kim IY, et al. Applications of stable, nonradioactive isotope tracers in in vivo human metabolic research. *Exp Mol Med*. 2016;48(1):e203.

35. Borén J, et al. Kinetic studies to investigate lipoprotein metabolism. *J Intern Med*. 2012;271(2):166–173.

36. Enkhmaa B, et al. Postprandial lipoproteins and cardiovascular disease risk in diabetes mellitus. *Curr Diab Rep*. 2010;10(1):61–69.

37. Higgins V, Adeli K. Postprandial dyslipidemia: pathophysiology and cardiovascular disease risk assessment. *EJIFCC*. 2017;28(3):168–184.

38. Romijn JA, et al. Substrate metabolism during different exercise intensities in endurance-trained women. *J Appl Physiol (1985)*. 2000;88(5):1707–1714.

39. Kim IY, et al. Acute lysine supplementation does not improve hepatic or peripheral insulin sensitivity in older, overweight individuals. *Nutr Metab (Lond)*. 2014;11(1):49.

40. Zheng C, et al. Metabolism of apoB lipoproteins of intestinal and hepatic origin during constant feeding of small amounts of fat. *J Lipid Res*. 2006;47(8):1771–1779.

41. Padilla N, et al. Effects of bariatric surgery on hepatic and intestinal lipoprotein particle metabolism in obese, nondiabetic humans. *Arterioscler Thromb Vasc Biol*. 2014;34(10):2330–2337.

42. Björnson E, et al. Investigation of human apoB48 metabolism using a new, integrated non-steady-state model of apoB48 and apoB100 kinetics. *J Intern Med*. 2019;285(5):562–577.

43. Griffo E, et al. Early improvement of postprandial lipemia after bariatric surgery in obese type 2 diabetic patients. *Obes Surg*. 2014;24(5):765–770.

44. Griffo E, et al. Effects of sleeve gastrectomy and gastric bypass on postprandial lipid profile in obese type 2 diabetic patients: a 2-year follow-up. *Obes Surg*. 2016;26(6):1247–1253.

45. Waldmann E, et al. Effect of sleeve gastrectomy on postprandial lipoprotein metabolism in morbidly obese patients. *Lipids Health Dis*. 2013;12(1):82.

46. Brunzell JD, et al. Evidence for a common, saturable, triglyceride removal mechanism for chylomicrons and very low density lipoproteins in man. *J Clin Invest*. 1973;52(7):1578–1585.

47. Cohn JS, et al. Contribution of apoB-48 and apoB-100 triglyceride-rich lipoproteins (TRL) to postprandial increases in the plasma concentration of TRL triglycerides and retinyl esters. *J Lipid Res*. 1993;34(12):2033–2040.

48. Van Beek AP, et al. Preferential clearance of apoB-48-containing lipoproteins after heparin- induced lipolysis is modulated by lipoprotein lipase activity. *J Lipid Res*. 1998;39(2):322–332.

49. Søndergaard E, et al. Postprandial VLDL-triacylglycerol secretion is not suppressed in obese type 2 diabetic men. *Diabetologia*. 2012;55(10):2733–2740.

50. Adiels M, et al. Postprandial accumulation of chylomicrons and chylomicron remnants is determined by the clearance capacity. *Atherosclerosis*. 2012;222(1):222–228.

51. Bjorkegren J, et al. Accumulation of large very low density lipoprotein in plasma during intravenous infusion of a chylomicron-like triglyceride emulsion reflects competition for a common lipolytic pathway. *J Lipid Res*. 1996;37(1):76–86.

52. Karpe F, Hultin M. Endogenous triglyceride-rich lipoproteins accumulate in rat plasma when competing with a chylomicron-like triglyceride emulsion for a common lipolytic pathway. *J Lipid Res*. 1995;36(7):1557–1566.

53. Kovrov O, et al. Lipoprotein size is a main determinant for the rate of hydrolysis by exogenous LPL in human plasma. *J Lipid Res*. 2022;63(1):100144.

54. Moreland AM, et al. Steatorrhea and hyperoxaluria in severely obese patients before and after Roux-en-Y gastric bypass. *Gastroenterology*. 2017;152(5):1055–1067.

55. Odstrcil EA, et al. The contribution of malabsorption to the reduction in net energy absorption after long-limb Roux-en-Y gastric bypass. *Am J Clin Nutr*. 2010;92(4):704–713.

56. Mahawar KK, Sharples AJ. Contribution of malabsorption to weight loss after Roux-en-Y gastric bypass: a systematic review. *Obes Surg*. 2017;27(8):2194–2206.

57. Carswell KA, et al. The effect of bariatric surgery on intestinal absorption and transit time. *Obes Surg*. 2014;24(5):796–805.

58. Kumar R, et al. Fat malabsorption and increased intestinal oxalate absorption are common after Rouxen-Y gastric bypass surgery. *Surgery*. 2011;149(5):654.

59. Haas ME, et al. The regulation of ApoB metabolism by insulin. *Trends Endocrinol Metab*. 2013;24(8):391–397.

60. Kamagate A, et al. FoxO1 mediates insulin-dependent regulation of hepatic VLDL production in mice. *J Clin Invest*. 2008;118(6):2347–2364.

61. Bartels ED, et al. Hepatic expression of microsomal triglyceride transfer protein and in vivo secretion of triglyceride-rich lipoproteins are increased in obese diabetic mice. *Diabetes*. 2002;51(4):1233–1239.

62. Sadur CN, Eckel RH. Insulin stimulation of adipose tissue lipoprotein lipase. Use of the euglycemic clamp technique. *J Clin Invest*. 1982;69(5):1119–1125.

63. Fried SK, et al. Lipoprotein lipase regulation by insulin and glucocorticoid in subcutaneous and omental adipose tissues of obese women and men. *J Clin Invest*. 1993;92(5):2191–2198.

64. Nadkarni P, et al. Regulation of glucose homeostasis by GLP-1. *Prog Mol Biol Transl Sci*. 2014;121:23–65.

65. Müller TD, et al. Glucagon-like peptide 1 (GLP-1). *Mol Metab*. 2019;30:72–130.

66. Holst JJ, et al. The role of incretins on insulin function and glucose homeostasis. *Endocrinology*. 2021;162(7):bqab065.

67. Farr S, et al. Glucagon-like peptide-1 as a key regulator of lipid and lipoprotein metabolism in fasting and postprandial states. *Cardiovasc Hematol Disord Drug Targets*. 2014;14(2):126–136.

68. Novodvorský P, Haluzík M. The effect of GLP-1 receptor agonists on postprandial lipaemia. *Curr Atheroscler Rep*. 2022;24(1):13–21.

69. Nahmias A, et al. GLP-1 (glucagon-like peptide-1) is physiologically relevant for chylomicron secretion beyond its known pharmacological role. *Arterioscler Thromb Vasc Biol*. 2021;41(6):1893–1900.

70. Farr S, et al. Central nervous system regulation of intestinal lipoprotein metabolism by glucagon-like peptide-1 via a brain-gut axis. *Arterioscler Thromb Vasc Biol*. 2015;35(5):1092–1100.

71. Taher J, et al. GLP-1 receptor agonism ameliorates hepatic VLDL overproduction and de novo lipogenesis in insulin resistance. *Mol Metab*. 2014;3(9):823–833.

72. Parlevliet ET, et al. GLP-1 receptor activation inhibits VLDL production and reverses hepatic steatosis by decreasing hepatic lipogenesis in high-fat-fed APOE*3-Leiden mice. *PLoS One*. 2012;7(11):e49152.

73. Khound R, et al. GLP-1 elicits an intrinsic gut-liver metabolic signal to ameliorate diet-induced VLDL overproduction and insulin resistance. *Arterioscler Thromb Vasc Biol*. 2017;37(12):2252–2259.

74. Jirapinyo P, et al. A meta-analysis of GLP-1 after Roux-En-Y gastric bypass: impact of surgical technique and measurement strategy. *Obes Surg*. 2018;28(3):615–626.

75. Hindsø M, et al. The role of GLP-1 in postprandial glucose metabolism after bariatric surgery: a narrative review of human GLP-1 receptor antagonist studies. *Surg Obes Relat Dis*. 2021;17(7):1383–1391.

76. Dar MS, et al. GLP-1 response to a mixed meal: what happens 10 years after Roux-en-Y gastric bypass (RYGB)? *Obes Surg*. 2012;22(7):1077–1083.

77. Martinussen C, et al. Augmented GLP-1 secretion as seen after gastric bypass may be obtained by delaying carbohydrate digestion. *J Clin Endocrinol Metab*. 2019;104(8):3233–3244.

78. Ten Kulve JS, et al. Elevated postoperative endogenous GLP-1 levels mediate effects of roux-en-Y gastric bypass on neural responsivity to food cues. *Diabetes Care*. 2017;40(11):1522–1529.

79. Miras AD, et al. The effect of standard versus longer intestinal bypass on GLP-1 regulation and glucose metabolism in patients with type 2 diabetes undergoing Roux-en-Y gastric bypass: the long-limb study. *Diabetes Care*. 2021;44(5):1082–1090.

80. Rhee NA, et al. Current evidence for a role of GLP-1 in Roux-en-Y gastric bypass-induced remission of type 2 diabetes. *Diabetes Obes Metab*. 2012;14(4):291–298.

81. Vidal J, Jiménez A. Diabetes remission following metabolic surgery: is GLP-1 the culprit? *Curr Atheroscler Rep*. 2013;15(10):357.

82. Klein S, et al. Gastric bypass surgery improves metabolic and hepatic abnormalities associated with nonalcoholic fatty liver disease. *Gastroenterology*. 2006;130(6):1564–1572.

83. Vargas V, et al. Surgically induced weight loss by gastric bypass improves non alcoholic fatty liver disease in morbid obese patients. *World J Hepatol*. 2012;4(12):382–388.

84. Cazzo E, et al. Effect of Roux-en-Y gastric bypass on nonalcoholic fatty liver disease evaluated through NAFLD fibrosis score: a prospective study. *Obes Surg*. 2015;25(6):982–985.

85. Matsuzaka T, Shimano H. Molecular mechanisms involved in hepatic steatosis and insulin resistance. *J Diabetes Investig*. 2011;2(3):170–175.

86. ter Horst KW, et al. Hepatic diacylglycerol-associated protein kinase Cε translocation links hepatic steatosis to hepatic insulin resistance in humans. *Cell Rep*. 2017;19(10):1997–2004.

87. Verdam FJ, et al. [Practice guideline for the treatment of morbid obesity]. *Ned Tijdschr Geneeskd*. 2012;156(23):A4630.

88. Demant T, et al. Sensitive methods to study human apolipoproteinB metabolism using stable isotope-labeled amino acids. *Am J Physiol Endocrinol Metab*. 1996;270(6 pt 1):E1022–E1036.

89. Bouter KEC, et al. The effect of dapagliflozin on apolipoprotein B and glucose fluxes in patients with type 2 diabetes and well-controlled plasma LDL cholesterol. *Diabetes Obes Metab*. 2020;22(6):988–996.

90. Van Den Akker CHP, et al. Human fetal albumin synthesis rates during different periods of gestation. *Am J Clin Nutr*. 2008;88(4):997–1003.

91. Ter Horst KW, et al. Insulin resistance in obesity can be reliably identified from fasting plasma insulin. *Int J Obes*. 2015;39(12):1703–1709.

92. Ter Horst KW, et al. Hepatic insulin resistance is not pathway selective in humans with nonalcoholic fatty liver disease. *Diabetes Care*. 2021;44(2):489–498.

93. Steele R. Influences of glucose loading and of injected insulin on hepatic glucose output. *Ann N Y Acad Sci*. 1959;82(2):420–430.

94. Finegood DT, et al. Estimation of endogenous glucose production during hyperinsulinemic-euglycemic glucose clamps. Comparison of unlabeled and labeled exogenous glucose infusates. *Diabetes*. 1987;36(8):914–924.

95. Ter Horst KW, et al. Impaired insulin action in the liver, but not in adipose tissue or muscle, is a distinct metabolic feature of impaired fasting glucose in obese humans. *Metabolism*. 2016;65(5):757–763.

96. Magkos F, Mittendorfer B. Stable isotope-labeled tracers for the investigation of fatty acid and triglyceride metabolism in humans in vivo. *Clin Lipidol*. 2009;4(2):215–230.

97. Ter Horst KW, et al. The FGF21 response to fructose predicts metabolic health and persists after bariatric surgery in obese humans. *Mol Metab*. 2017;6(11):1493–1502.

98. Van Der Valk F, et al. The effect of a diiodothyronine mimetic on insulin sensitivity in male cardiometabolic patients: a double-blind randomized controlled trial. *PLoS One*. 2014;9(2):e86890.